Resource

Cell Reports

Optical Dissection of Experience-Dependent Pre- and Postsynaptic Plasticity in the *Drosophila* Brain

Graphical Abstract

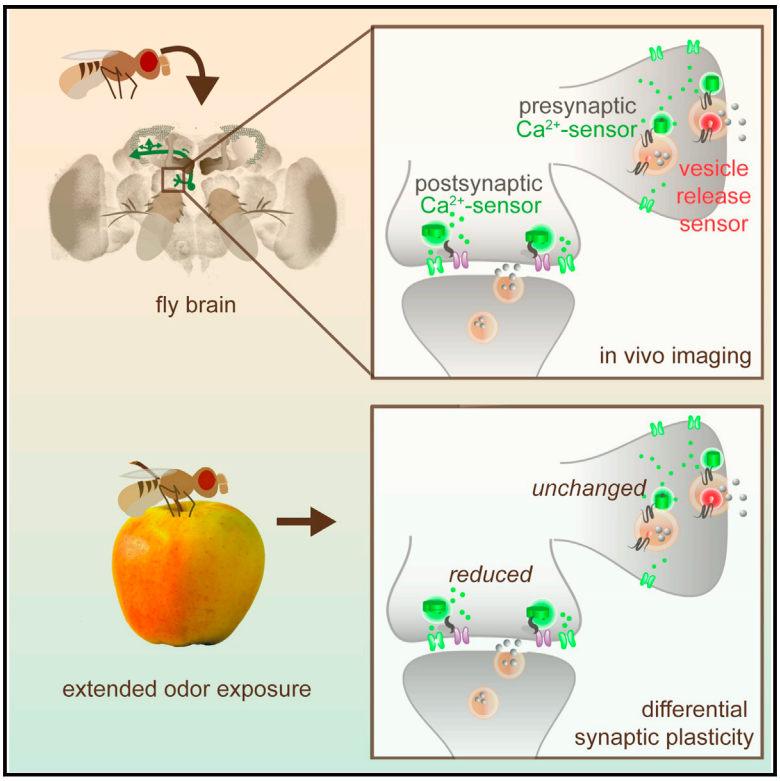

Authors

Ulrike Pech, Natalia H. Revelo, ..., Silvio O. Rizzoli, André Fiala

Correspondence

afiala@gwdg.de

In Brief

Drosophila is a favorable organism for analysis of genetic and neuronal mechanisms underlying learning and memory. Pech et al. report an optical approach to selectively monitor pre- and postsynaptic activity. They thus dissect experience-dependent pre- and postsynaptic plasticity in the intact *Drosophila* brain.

Highlights

- Transgenic *Drosophila* strains expressing synaptic sensors are reported
- Concurrent dual color imaging of pre- and postsynaptic activity is demonstrated
- Olfactory coding across synapses is visualized in central olfactory neurons
- Experience-dependent pre- and postsynaptic plasticity is differentiated

Pech et al., 2015, Cell Reports *10*, 2083–2095
March 31, 2015
http://dx.doi.org/10.1016/j.celrep.2015.02.065

CellPress

Cell Reports
Resource

Optical Dissection of Experience-Dependent Pre- and Postsynaptic Plasticity in the *Drosophila* Brain

Ulrike Pech,[1] Natalia H. Revelo,[2] Katharina J. Seitz,[2] Silvio O. Rizzoli,[2] and André Fiala[1,*]
[1]Department of Molecular Neurobiology of Behavior, Johann-Friedrich-Blumenbach-Institute for Zoology and Anthropology, Georg-August-University Göttingen, Julia-Lermontowa-Weg 3, 37077 Göttingen, Germany
[2]Department of Neuro- and Sensory Physiology, University of Göttingen Medical Center, Humboldtallee 23, 37073 Göttingen, Germany
*Correspondence: afiala@gwdg.de
http://dx.doi.org/10.1016/j.celrep.2015.02.065

SUMMARY

Drosophila **represents a key model organism for dissecting neuronal circuits that underlie innate and adaptive behavior. However, this task is limited by a lack of tools to monitor physiological parameters of spatially distributed, central synapses in identified neurons. We generated transgenic fly strains that express functional fluorescent reporters targeted to either pre- or postsynaptic compartments. Presynaptic Ca^{2+} dynamics are monitored using synaptophysin-coupled GCaMP3, synaptic transmission is monitored using red fluorescent synaptophysin-pHTomato, and postsynaptic Ca^{2+} dynamics are visualized using GCaMP3 fused with the postsynaptic matrix protein, *d*Homer. Using two-photon in vivo imaging of olfactory projection neurons, odor-evoked activity across populations of synapses is visualized in the antennal lobe and the mushroom body calyx. Prolonged odor exposure causes odor-specific and differential experience-dependent changes in pre- and postsynaptic activity at both levels of olfactory processing. The approach advances the physiological analysis of synaptic connections across defined groups of neurons in intact *Drosophila*.**

INTRODUCTION

Monitoring of neuronal activity is crucial for the functional analysis of distinct neuronal circuits. Optical approaches provide an advantage over electrophysiological techniques for recording spatio-temporal activity across neuronal populations without mechanical interference. With the invention of genetically encoded fluorescent reporter proteins (reviewed by Tantama et al., 2012), the corresponding sensors can be expressed reproducibly in specific neurons of interest. Therefore, transgenic model organisms, e.g., mice, *Caenorhabditis elegans*, *Danio rerio*, or *Drosophila melanogaster*, are of predominant significance in neuroscience.

Drosophila represents a favorable organism due to the versatility of genetic tools with which expression of transgenes, including reporter proteins, can be restricted to defined populations of neurons (Venken et al., 2011). Imaging neuronal activity in correlation with sensory stimuli or with behavioral actions using genetically encoded Ca^{2+} indicators (GECIs) represents a widely applied approach (Riemensperger et al., 2012). Typically, GECIs are expressed in the entire neuronal cytosol. Therefore, they report changes in the dynamics of cytosolic Ca^{2+} ions as integrated signals (Grienberger and Konnerth, 2012). Intracellular Ca^{2+} ions have many different sources and different physiological functions. Synaptic connections represent key elements underlying neuronal signal integration, processing, and plasticity. Therefore, techniques are required with which to restrict the analysis to either pre- or postsynaptic activity. This is of particular importance if neuronal activity is monitored in the dense neuropils of the central brain that often comprise various pre- and postsynaptic elements in close proximity. Whereas GECIs targeted specifically to presynapses have been developed for and applied in the nervous systems of some vertebrates (Dreosti et al., 2009; Li et al., 2011), no equivalent technique exists yet for the *Drosophila* brain. Here, we report the generation and characterization of transgenic *Drosophila* strains that express the Ca^{2+} sensor, GCaMP3 (Tian et al., 2009), targeted either to the presynapse or the postsynapse. In addition, we generated a fly strain that expresses the red fluorescent reporter of synaptic vesicle release, pHTomato (Li and Tsien, 2012), inserted into an intravesicular domain of Synaptophysin. In combination with the green fluorescent, synaptically targeted GECIs, vesicle release and either pre- or postsynaptic Ca^{2+} dynamics can be monitored simultaneously. We use this approach to dissect odor-evoked pre- and postsynaptic neuronal activity in olfactory projection neurons of the central brain, and we demonstrate odor-specific and differential experience-dependent changes in synaptic activity.

RESULTS

Targeting Fluorescent Sensors to Synapses in the *Drosophila* Central Brain

For monitoring presynaptic Ca^{2+}, we used a fusion construct that is functional in vertebrates, i.e., the GCaMP3 linked to the

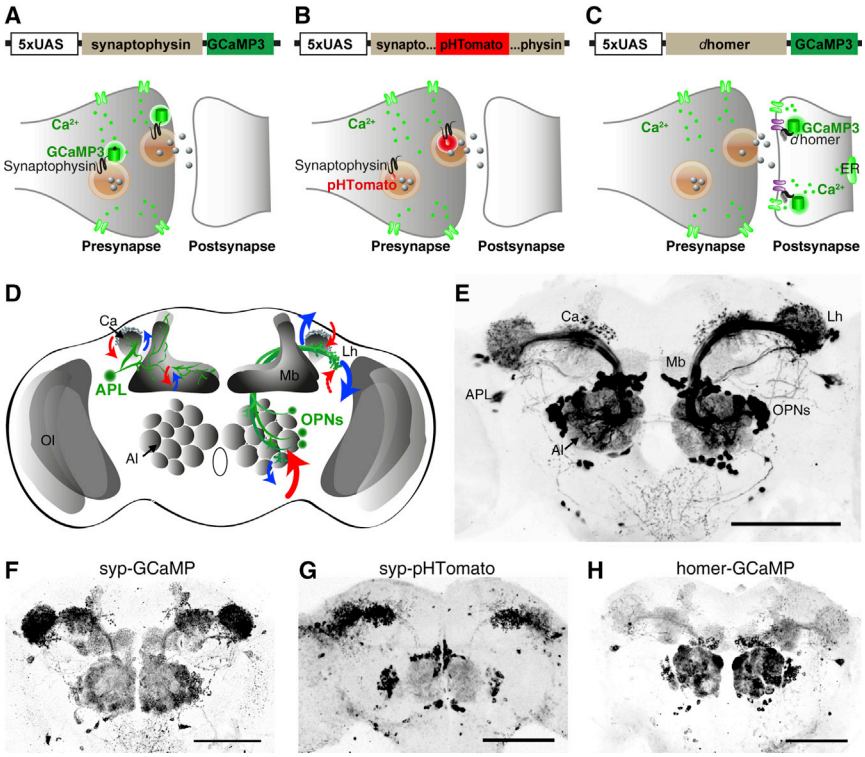

Figure 1. Synaptically Targeted Sensors and Their Differential Expression in Olfactory Projection Neurons

(A) GCaMP3 is targeted to the cytoplasmic site of synaptic vesicles by linking to the C terminus of rat Synaptophysin.

(B) pHTomato is targeted to the lumen of synaptic vesicles by insertion into the first intravesicular domain of rat Synaptophysin.

(C) GCaMP3 is targeted to postsynaptic densities by linking to the C terminus of *d*Homer.

(D) Schematic depiction of the *Drosophila* brain. Neurons targeted by GH146-Gal4 are highlighted in green (anterior paired lateral neuron innervating the mushroom body on the left [APL] and olfactory projection neurons on the right [OPNs]). Red arrows indicate postsynaptic sites and blue arrows presynaptic sites, and the weight of arrows indicates their proportions.

(E) Anti-GFP immunostaining of a *Drosophila* brain expressing cytosolic GCaMP3 under control of GH146-Gal4.

(F) Anti-GFP immunostaining of synaptophysin-GCaMP3.

(G) Anti-RFP immunostaining of synaptophysin-pHTomato.

(H) Anti-GFP immunostaining of *d*homer-GCaMP3. Immunohistochemical stainings (E–G) show projections of maximal fluorescence intensity across a stack of confocal images. Al, antennal lobe; Ca, mushroom body calyx; Lh, lateral horn; Mb, mushroom body lobes; Ol, optical lobe; scale bars 100 μm. See also Figures S1 and S2.

cytoplasmic C terminus of the rat Synaptophysin protein (Dreosti et al., 2009; Li et al., 2011) (Figure 1A). Fruit flies do not endogenously express a Synaptophysin homolog. Nevertheless, this protein shows specific self-assembly in the membrane of synaptic vesicles when it is ectopically expressed (Leube, 1995). To monitor synaptic transmission concurrently, we inserted the red fluorescent pH-sensor pHTomato into the first intravesicular domain of Synaptophysin (Li and Tsien, 2012) (Figure 1B). To target the GECI to the postsynaptic densities of neurons, we linked GCaMP3 with the C terminus of the *Drosophila* Homer protein. *d*Homer is a homolog of the PDZ-domain-containing Homer proteins of vertebrates, sharing equivalent subcellular localization and conserved binding motifs, and it is expressed in all neurons of the *Drosophila* nervous system (Xiao et al., 1998; Diagana et al., 2002) (Figure 1C). Transgenic flies were generated that express these DNA constructs under control of upstream activator sequences (UASs) (Brand and Perrimon, 1993).

To probe the efficiency of the constructs in neurons of the fly central brain, we used the well-characterized GH146-Gal4 driver line (Stocker et al., 1997), which induces gene expression in two populations of central neurons. GH146-Gal4 targets ~83 olfactory projection neurons (OPNs) that project from the antennal lobe (AL), the primary olfactory neuropil of the insect brain, to the calyx (CA) of the mushroom body (MB) and the lateral horn (LH) (Stocker et al., 1997; Wong et al., 2002) (Figure 1D). OPNs receive their main postsynaptic input in the glomeruli of the AL but also exhibit some presynaptic output in this neuropil (Ng et al., 2002; Wilson et al., 2004). The majority of their axons form the inner antennocerebral tract that terminates in the LH. Short axonal collaterals furnished with large synaptic boutons innervate the CA of the MB and provide mostly presynaptic output to intrinsic MB neurons (Kenyon cells), but they also receive some postsynaptic input (Yasuyama et al., 2002; Christiansen et al., 2011; Butcher et al., 2012). In addition, GH146-Gal4 targets large interneurons (anterior paired lateral [APL] neurons) that recurrently innervate the MB neuropil, although expression in those neurons is weak when compared to OPNs (see Figure 1E). The expression patterns of the targeted sensors indicate correct targeting of the sensor proteins to synaptic terminals in accordance with the described polarity of the neurons, as presynaptic sensors are enriched at the main output sites, CA and LH (Figures 1F and 1G), and homer-GCaMP is enriched at the main OPN input site, the AL (Figure 1H).

To detail the localization of the sensors, we analyzed the CA and the AL and calculated the ratio of immunohistochemical staining intensity in synaptic terminals to that in axons. Cytosolic GCaMP is equally present both in synaptic structures and axonal tracts. In contrast, all three synaptic sensors localize in a manner comparable to the presynaptic marker, anti-synaptotagmin (anti-syt), or the postsynaptic marker, anti-discs large (anti-DLG) (Figures 2A and 2B). We also confirmed proper synaptic targeting by focusing on the predominantly presynaptic boutons in the CA (Figure 2C). In contrast to cytosolic GCaMP, synaptophysin-GCaMP (syp-GCaMP) and synaptophysin-pHTomato (syp-pHTomato) are strongly confined to these boutons,

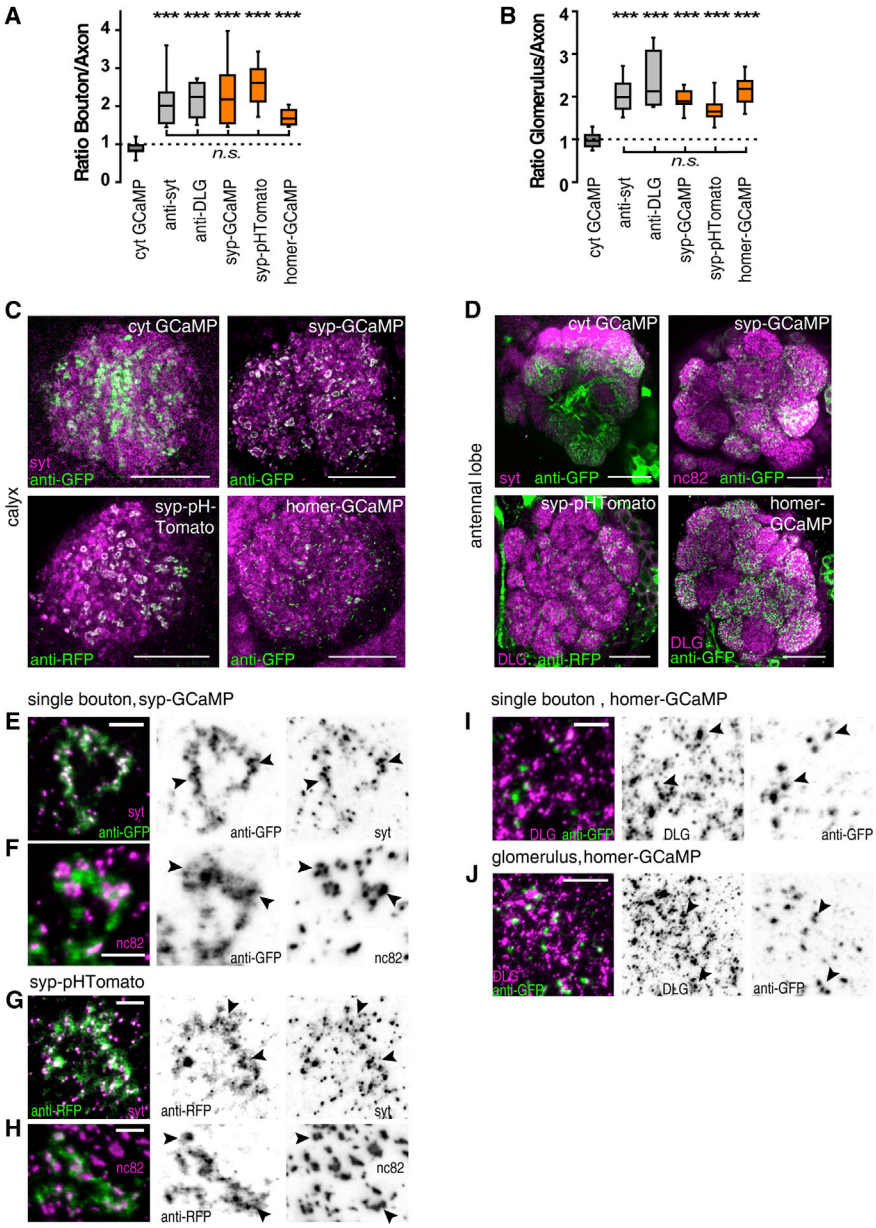

Figure 2. Synaptic Localization of the Fluorescent Sensors

(A) Quantification of immunostaining intensity of the fluorescent sensors in synaptic boutons of OPNs in the mushroom body calyx compared with the intensity in adjacent axonal tracts. The ratio is compared to that of the presynaptic vesicle protein Synaptotagmin (anti-syt) and the postsynaptic protein discs-large (anti-DLG). $n \geq 10$ calyces.

(B) Same as in (A) for the glomeruli of the antennal lobe (AL). $n \geq 10$ ALs. Box plots indicate medians, interquartile ranges, and 10%/90% range. *n.s.*, $p > 0.05$; two-sample t test; ***$p < 0.001$ Wilcoxon signed rank test.

(C) Immunostaining of cytosolic GCaMP, syp-GCaMP, syp-pHTomato, and homer-GCaMP in the calyx. Shown are anti-syt immunoreactivity and anti-GFP or anti-RFP immunoreactivity.

(D) Immunostaining of cytosolic GCaMP, syp-GCaMP, syp-pHTomato, and homer-GCaMP in the AL. Shown are synaptic co-stainings and anti-GFP or anti-RFP immunoreactivity.

(E–I) High-resolution STED microscopy images of a single bouton in the calyx. Shown are a merge and the individual channels of anti-GFP immunoreactivity of syp-GCaMP and either anti-syt immunoreactivity (E) or immunoreactivity against the active zone protein Bruchpilot (nc82) (F). Immunoreactivity of syp-pHTomato and either anti-syt immunoreactivity (G) or immunoreactivity against Bruchpilot (nc82) (H). Arrowheads point to regions of co-localization in clusters of vesicles.

(I) Shown are a merge, anti-DLG immunoreactivity, and anti-GFP immunoreactivity of homer-GCaMP.

(J) High-resolution detail within a glomerulus of the AL, shown as a merge, and individual anti-DLG immunoreactivity and anti-GFP immunoreactivity of homer-GCaMP. Arrowheads point to co-localization.

The scale bars represent 20 μm in (C) and (D), 1 μm in (E)–(I), and 2 μm in (J).

whereas homer-GCaMP punctae are diffusely distributed across the CA (Figure 2C) in accordance with the microanatomy of calycal boutons (Yasuyama et al., 2002; Leiss et al., 2009; Butcher et al., 2012). In addition, this staining pattern might partly reflect postsynapses of the APL neuron in the CA. Furthermore, we analyzed the localization of all constructs in the main OPN input region, the AL. Cytosolic GCaMP is present throughout neuronal ramifications within the AL, whereas the presynaptically targeted sensors are confined to irregularly shaped and heterogeneously distributed punctae within the AL's glomeruli (Figure 2D). By contrast, homer-GCaMP is localized to punctae that are not only much more numerous but also smaller and more densely distributed, in accordance with the fine mesh of dendritic processes pervading the glomeruli (Figure 2D). To visualize the subcellular localization of the sensors, we used high resolution STED microscopy (Figures 2E–2J). Within individual boutons in the CA, an accumulation of syp-GCaMP or of syp-pHTomato punctae was evident in distinct regions (Figures 2G and 2J). These punctae reflect the accumulation of synaptic vesicles at active zones as they co-localize with anti-syt immunoreactivity (Figures 2E and 2G). In addition, they are localized around and partially co-localize with immunoreactivity against the active zone protein Bruchpilot (Wagh et al., 2006) (Figures 2F and 2H). These data confirm that both synaptophysin-coupled constructs are targeted to presynaptic vesicles. STED microscopy analysis further revealed that homer-GCaMP punctae are directly adjacent to or co-localize with anti-DLG, both in the CA (Figure 2I) and the AL (Figure 2J). In conclusion, homer-GCaMP localizes to substructures of the complex postsynaptic matrix. We also confirmed the correct localization of the three sensors in motor neurons of the larval body wall. Again, syp-GCaMP and syp-pHTomato are located presynaptically in the boutons of neuromuscular junctions and co-localize with anti-syt immunoreactivity (Figures S1A and S1B). In contrast, homer-GCaMP is absent from presynaptic boutons but is detected in dendritic structures of motor neurons within the ventral ganglion of the larval CNS (Figure S1C).

To test whether the expression of the sensors affects the morphology of synaptic boutons, we expressed the constructs in larval motor neurons and determined the number and size of boutons at NMJ6/7 in segment A3 using anti-DLG or anti-syt immunostaining (Figure S1D). No differences in either the number or size of both type Ib and type Is boutons were observed when compared to w1118 larvae (Figure S1E). To further test whether the sensors cause any functional impairment, we expressed the constructs ubiquitously in all cells and quantified synaptic vesicle recycling via FM (styryl) dye uptake and release (Kuromi and Kidokoro, 1999). FM dye is taken up during stimulation and therefore serves as a measure for the size of the vesicle population that undergoes recycling. Further stimulation in absence of the dye releases it from these vesicles (termed FM destaining), thereby providing an estimate for the exocytosis kinetics. Neither synaptic targeting of GCaMP nor syp-pHTomato expression altered FM dye uptake compared to the respective controls (Figure S1F). FM dye destaining was also unaffected (Figure S1G). We further tested the performance of such animals in two behavioral assays. We found neither an overall morphological aberration of larvae (Figure S2A) nor a behavioral deficit in a larval chemotaxis assay (Figure S2B). Moreover, the morphology of adult animals and their brains were indistinguishable from those of control animals and the flies behaved normally in a negative geotaxis assay (Figures S2C and S2D). In conclusion, we did not detect any interference of the three constructs with neuronal function.

Functionality of the Synaptic Sensors

To compare the functionality of the synaptic sensors in reporting pre- or postsynaptic Ca^{2+} influx, or vesicle exocytosis, we expressed the DNA constructs in OPNs and used in vivo wide-field imaging to monitor the fluorescence within the entire AL and CA neuropils. KCl-induced neuronal depolarization caused clear increases in fluorescence emission in either sensor (Figure S3). The relative changes in fluorescence intensity of syp-GCaMP exceeded that of cytosolic GCaMP3, whereas homer-GCaMP showed smaller signal amplitudes when compared to cytosolic GCaMP (Figures S3A and S3B). Because all GECIs share the same Ca^{2+} sensor and differ only in their subcellular localization, the differential amplitudes reflect differential contributions from sources of Ca^{2+} influx in pre- and postsynaptic compartments. The red syp-pHTomato displayed relative changes in fluorescence and a signal-to-noise ratio within a similar range when compared with synaptopHluorin (Ng et al., 2002) (Figure S3C).

Two-Photon Imaging of Odor-Induced Synaptic Activity

We next tested whether the synaptically targeted sensors can be used to monitor synaptic activity induced by physiological, sensory stimuli in largely intact animals. Odor-induced activity of presynaptic boutons of OPNs in the CA was monitored using two-photon microscopy. The baseline fluorescence of both synaptophysin-coupled sensors clearly demarcated individual presynaptic boutons (Figures S4A and S4F). The animals were stimulated with methyl cyclohexanol (MCH) and 3-octanol (3Oct) while monitoring either Ca^{2+} transients or synaptic vesicle release. Syp-GCaMP reliably reported presynaptic Ca^{2+} influx, and syp-pHTomato reliably reported increased vesicle exocytosis, both across many synapses and at the subcellular level (Figures S4A–S4J; Movie S1). The odor-induced fluorescence change of both sensors was characterized by a sharp peak upon odor onset, followed by decay already as soon as during odor stimulation (Figures S4D and S4I), and some boutons responded specifically to odor offset (Figures S4B, S4C, and S4H). Odor on- and offset Ca^{2+} transients in mutually exclusive OPNs might be attributed to a release of inhibition via recurrent interneurons in the AL (Silbering et al., 2008) and/or direct feedback from the LH and the MB lobes to the calycal boutons. The spatiotemporal, combinatorial nature of odor representations across OPNs (Wilson, 2013) is, therefore, reflected also at the level of presynaptic activity. As syp-pHTomato displayed increased fluorescence at few and distinct regions at the borders of individual boutons (Figure S4J), it provides a tool to visualize transmission events that are spatially confined to individual active zones in a given focal plane.

To record postsynaptic odor representations using homer-GCaMP, we focused on the AL. Baseline fluorescence clearly demarcated individual glomeruli (Figure S4K). Homer-GCaMP reported odor-induced Ca^{2+} transients reliably in postsynapses

within overlapping subsets of glomeruli (Figures S4K–S4M). In addition to Ca^{2+} transients induced by odor onset, homer-GCaMP also reported spontaneous Ca^{2+} activity (Movie S2) and Ca^{2+} transients induced by odor offset signaling (e.g., glomerulus DL1 shown in Figures S4L and S4M). These complex activation patterns of distinct glomeruli were stereotypic across individuals in terms of the amplitudes and kinetics of odor-evoked responses (e.g., glomerulus DL4 shown in Figure S4N).

Concurrent Imaging of Presynaptic Ca^{2+} Dynamics and Synaptic Transmission

Next, we tested whether syp-GCaMP and syp-pHTomato can be used to monitor two physiological parameters simultaneously. We co-expressed both constructs in OPNs and focused again on presynaptic boutons in the CA. Immunohistochemical staining confirmed that both constructs were targeted to the same boutons (Figure 3A). The fluorescence emitted by the two sensors co-localized completely in vivo as well, although baseline fluorescence intensities differed slightly across distinct boutons (Figure 3B). We analyzed comparatively the fluorescence emission changes of both reporters in response to the odors, MCH and 3Oct, in individual presynaptic boutons (Figures 3C and 3D). Syp-GCaMP and syp-pHTomato showed odor-induced increases in fluorescence emission in equivalent boutons. The exact kinetics of fluorescence changes, however, differed between the two emission wavelengths, as expected for the different properties of the sensors and the parameters measured (Figures 3C and 3D).

We focused next on OPN presynapses in the AL, where the stereotypic neuronal connectivity across individuals allowed the comparison of identical neurons with respect to their odor-response profiles, i.e., identifiable glomeruli. Both presynaptic constructs co-localize in the AL, which was confirmed with immunohistochemical labeling and was also visible in vivo (Figures 3E and 3F). Both reporters showed odor-induced increases in fluorescence emission, as shown for glomerulus DL4 (Figure 3G). Again, the overall odor-induced glomerular activity patterns, the relative amplitudes, and the time courses were a close match in presynaptic Ca^{2+} and synaptic transmission (Figure 3H). Baseline fluctuations of syp-pHTomato emission differed between glomeruli, indicating that different OPNs exhibit different spontaneous vesicle release rates. The VA1 glomerulus, for example, showed comparably high spontaneous vesicle exocytosis that was reduced during odor presentations (Figure 3H). In order to characterize the relation between presynaptic Ca^{2+} and vesicle release, we analyzed MCH-induced signals in the DL4 glomerulus in detail. The relation between syp-pHTomato and syp-GCaMP signals could most accurately be described by the sigmoid function $y = a1 + (a2 - a1)/(1 + 10^{(\log x0 - x)\,p})$ (Figure 3I). The obtained function also described the fluorescence signals induced by the different odors in the same glomerulus (Figure 3I) and reflected different phases of stimulus-induced activity. The slope of the bottom asymptote indicates basal fluctuations of the pHTomato signal, e.g., spontaneous transmitter release. The fact that there is a top asymptote reflects that transmitter release persists on top of elevated activity. This indicates that we optically recorded synaptic activity within the dynamic ranges of the sensors and that the odor responses recorded were below a range in which vesicle pool size and recruitment become limiting factors.

Concurrent Imaging of Postsynaptic Ca^{2+} and Presynaptic Vesicle Release

Next, we combined the syp-pHTomato with homer-GCaMP and co-expressed both sensors in OPNs, again focusing on the AL. Homer-GCaMP and syp-pHTomato were spatially segregated from each other. Only very rarely was co-localization detected (Figure 4A), although both constructs were targeted to the same set of glomeruli. The separated localization at only marginally overlapping structures was also observed with the in vivo baseline fluorescence and became most obvious when focusing on subglomerular structures in individual glomeruli, e.g., DL4 (Figures 4B and 4C). OPNs innervating DL4 respond to both MCH and 3Oct, with both postsynaptic Ca^{2+} increase and presynaptic vesicle exocytosis (Figure 4D). When all glomeruli within this focal plane were analyzed, the odor-induced combinatorial activity pattern, the relative amplitudes, and duration of glomerular activation of postsynaptic Ca^{2+} and presynaptic transmission were a close match in most cases (Figures 4D and 4E). Similarly as with presynaptic Ca^{2+} transients, the relation between postsynaptic Ca^{2+} and presynaptic vesicle release within the same neurons is best described by a sigmoid function (Figure 4F).

To further substantiate that syp-pHTomato reliably reports vesicle exocytosis independently of co-expressed Ca^{2+} sensors, we expressed syp-pHTomato and homer-GCaMP together with temperature-dependent $shibire^{ts}$ (Kitamoto, 2001) to disrupt vesicle-recycling reversibly. Switching the temperature at the fly's brain to the restrictive temperature of $shibire^{ts}$ diminished odor-induced syp-pHTomato signals while leaving homer-GCaMP signals unaffected (Figure S5). These experiments demonstrate that homer-GCaMP and syp-pHTomato can be used concurrently to differentiate, spatially and functionally, pre- and postsynaptic signaling within the same neurons, even in such dense aggregations of synapses as a glomerulus of the AL.

Differential Experience-Dependent Synaptic Plasticity in the AL

We asked whether the targeted sensors can be used to detect experience-dependent, physiological plasticity at synapses of the central brain. As a first step, we used artificial, chronic deprivation of synaptic transmission, which has been shown to induce structural changes at OPN synapses (Kremer et al., 2010). We restricted the artificially induced block of synaptic transmission to the flies' post-eclosion stage and used heat-sensitive $shibire^{ts}$ to transiently prevent vesicle recycling of OPNs for 5 days after eclosion. Subsequently, flies recovered at the permissive temperature and we then imaged the responses of the synaptically targeted sensors to two monomolecular odors and two complex blends of fruit in the AL and the CA (Figures 5 and 6) at the permissive temperature. In the AL, we compared odor responses in glomeruli DC1, DM3, and DL5, which respond to MCH, 3Oct, and apple and banana, respectively, using either a dual color combination of pre- or postsynaptic Ca^{2+} sensors and syp-pHTomato (Figures 5A

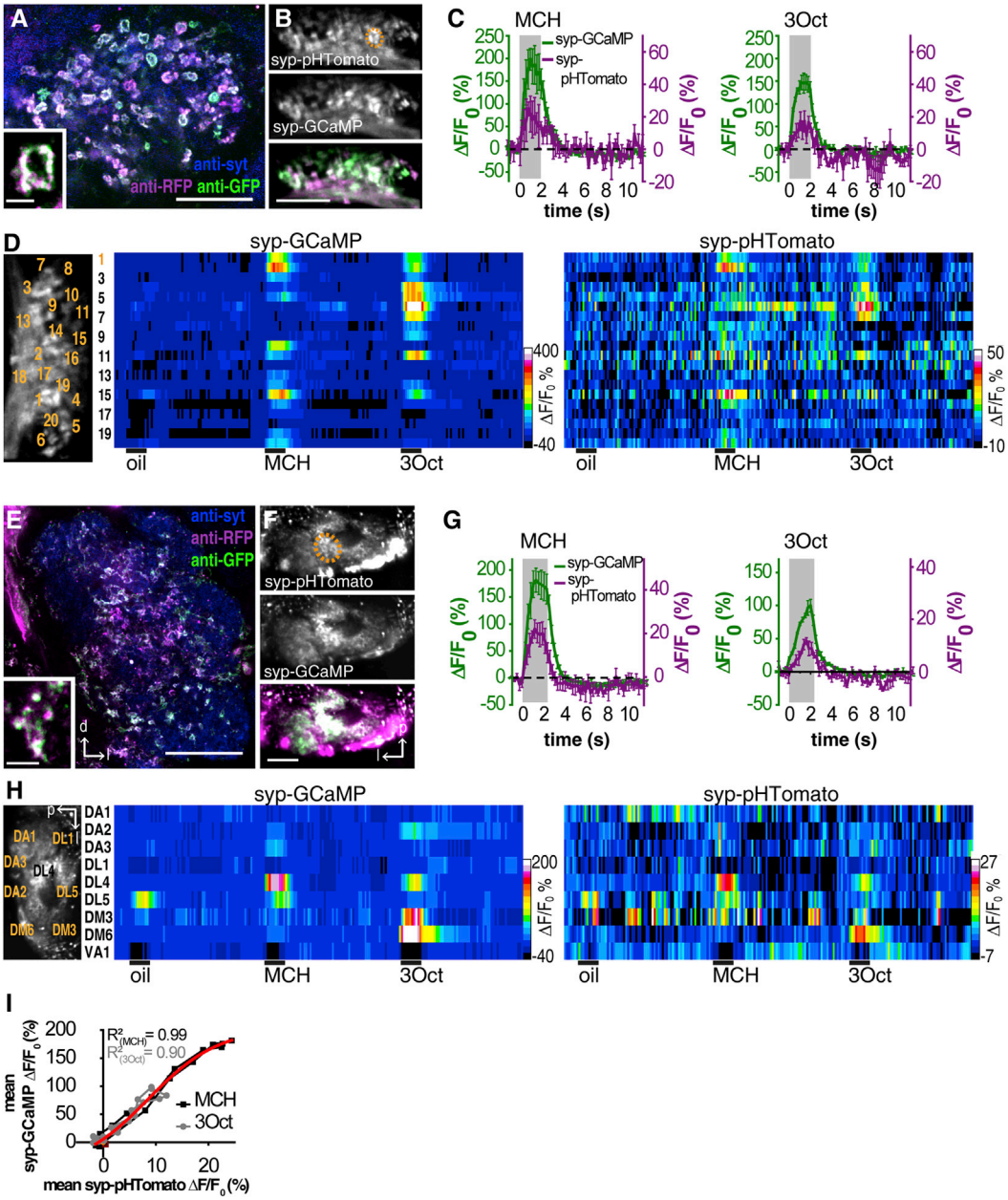

Figure 3. Concurrent Imaging of Presynaptic Ca^{2+} and Vesicle Release

(A) Co-expression of syp-GCaMP and syp-pHTomato in calycal boutons of OPNs. Blue, anti-synaptotagmin; magenta, syp-pHTomato detected by anti-RFP; green, syp-GCaMP detected by anti-GFP. The inset shows a magnification of one bouton; white color indicates co-localization.

(B) In vivo fluorescence of syp-pHTomato and syp-GCaMP in OPNs within the calyx.

(C) Odor-induced fluorescence change of syp-GCaMP (green) and syp-pHTomato (magenta) in one individual bouton (indicated by orange circle in B).

(D) Dynamics of fluorescence changes of syp-GCaMP (left) and syp-pHTomato (right) in 20 individual boutons. Each row of the heatmaps represents one bouton, each column one 200-ms time frame.

(E) Co-expressed syp-GCaMP and syp-pHTomato in the AL. The inset shows a magnification within one glomerulus; white color indicates co-localization.

(F) In vivo fluorescence of syp-pHTomato and syp-GCaMP. Glomerulus DL4 is indicated by the orange circle.

(G) Odor-induced fluorescence change of syp-GCaMP (green) and syp-pHTomato (magenta) in DL4.

(H) Fluorescence changes over time of syp-GCaMP (left) and syp-pHTomato (right) in nine glomeruli. Each row represents one glomerulus, each column one 250-ms time frame.

(I) The gray and black lines indicate the time course of fluorescence change in syp-GCaMP as a function of fluorescence change in syp-pHTomato during odor stimulation in DL4. The red line shows the sigmoid fit with the adjusted R^2 values for MCH and 3Oct. Heatmaps display the mean, traces the mean, and SEM of three stimulations.

d, dorsal; l, lateral; p, posterior; scale bars: 20 μm; in insets: 2 μm.

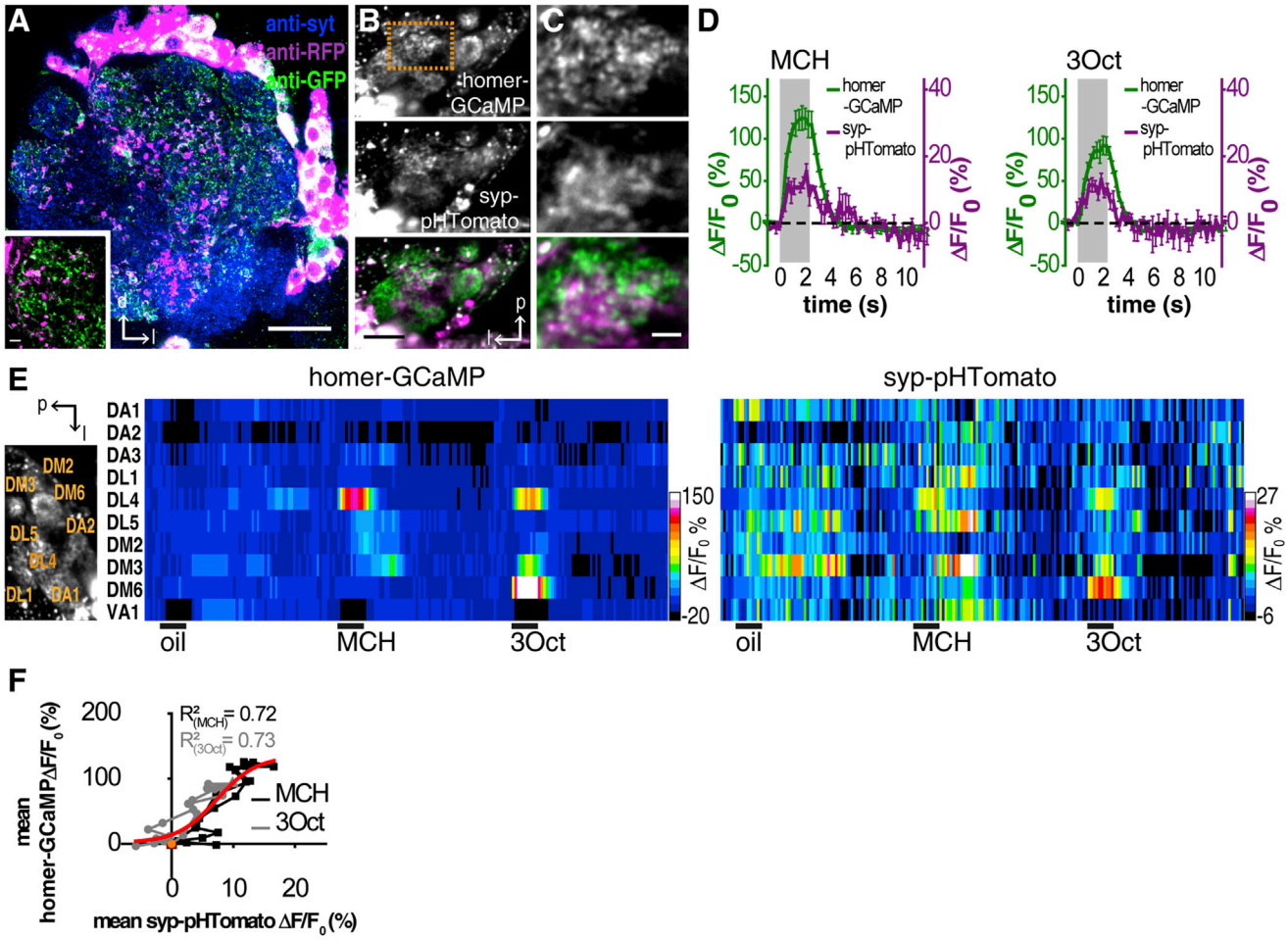

Figure 4. Concurrent Imaging of Postsynaptic Ca^{2+} and Vesicle Release

(A) Co-expression of homer-GCaMP and syp-pHTomato in OPNs in the AL. Blue, anti-syt; magenta, syp-pHTomato detected by anti-RFP; green, homer-GCaMP detected by anti-GFP. The inset shows a magnification of one glomerulus; white color indicates regions of co-localization.

(B) Individual and merged in vivo syp-pHTomato and homer-GCaMP fluorescence in OPNs in the AL.

(C) DL4 is indicated in orange and magnified.

(D) Odor-induced fluorescence change of homer-GCaMP (green) and syp-pHTomato (magenta) in DL4 (mean and SEM of three stimulations).

(E) Dynamics of fluorescence changes over time of homer-GCaMP (left) and syp-pHTomato (right) in ten glomeruli. Each row of the heatmaps represents one glomerulus, each column one 250-ms time frame. Pixel values represent the mean of three stimulations.

(F) Relation of dynamic fluorescence changes of homer-GCaMP and syp-pHTomato evoked by MCH and 3Oct. The red line shows a sigmoid fit across data points in DL4, with the adjusted R^2 values displayed for MCH and 3Oct.

The scale bars represent 20 μm in (A) and (B) and 2 μm in the insets (A) and (C). See also Figure S5.

and 5B). Odor-induced synaptic signaling was compared to siblings that were raised in parallel at the restrictive temperature but that did not express shibire^{ts}. As a further control, we raised animals with or without shibire^{ts} expression at the permissive temperature (Figure 5C). The 5-day deprivation of synaptic output did not lead to any alteration in presynaptic Ca^{2+} signaling of OPNs in the AL (Figure 5D) but reduced drastically the amplitudes of postsynaptic Ca^{2+} transients (Figure 5E). Vesicle exocytosis was not altered under any experimental condition, although we found that animals that expressed shibire^{ts} showed a slight, but not significant, reduced transmission when raised at either the restrictive or the permissive temperature (Figure 5F). Although presynaptic Ca^{2+} signaling was not altered in the AL, when focusing on individual boutons of the main OPN output site in the CA, syp-GCaMP reported significantly reduced presynaptic Ca^{2+} signaling evoked by all four odorants used (Figures 6A–6C). This indicates that presynaptic Ca^{2+} dynamics within spatially separated domains in different neuropils, but in the same neurons, can be modulated independently. In contrast, altered vesicle exocytosis monitored using syp-pHTomato was not detectable in the CA under any experimental condition (Figure 6D). A more-detailed analysis of boutons in the CA revealed that the prolonged deprivation of synaptic transmission from OPNs led to increased bouton sizes, which is in accordance with the findings of Kremer et al. (2010) (Figure 6E). We did not find any difference in the relative

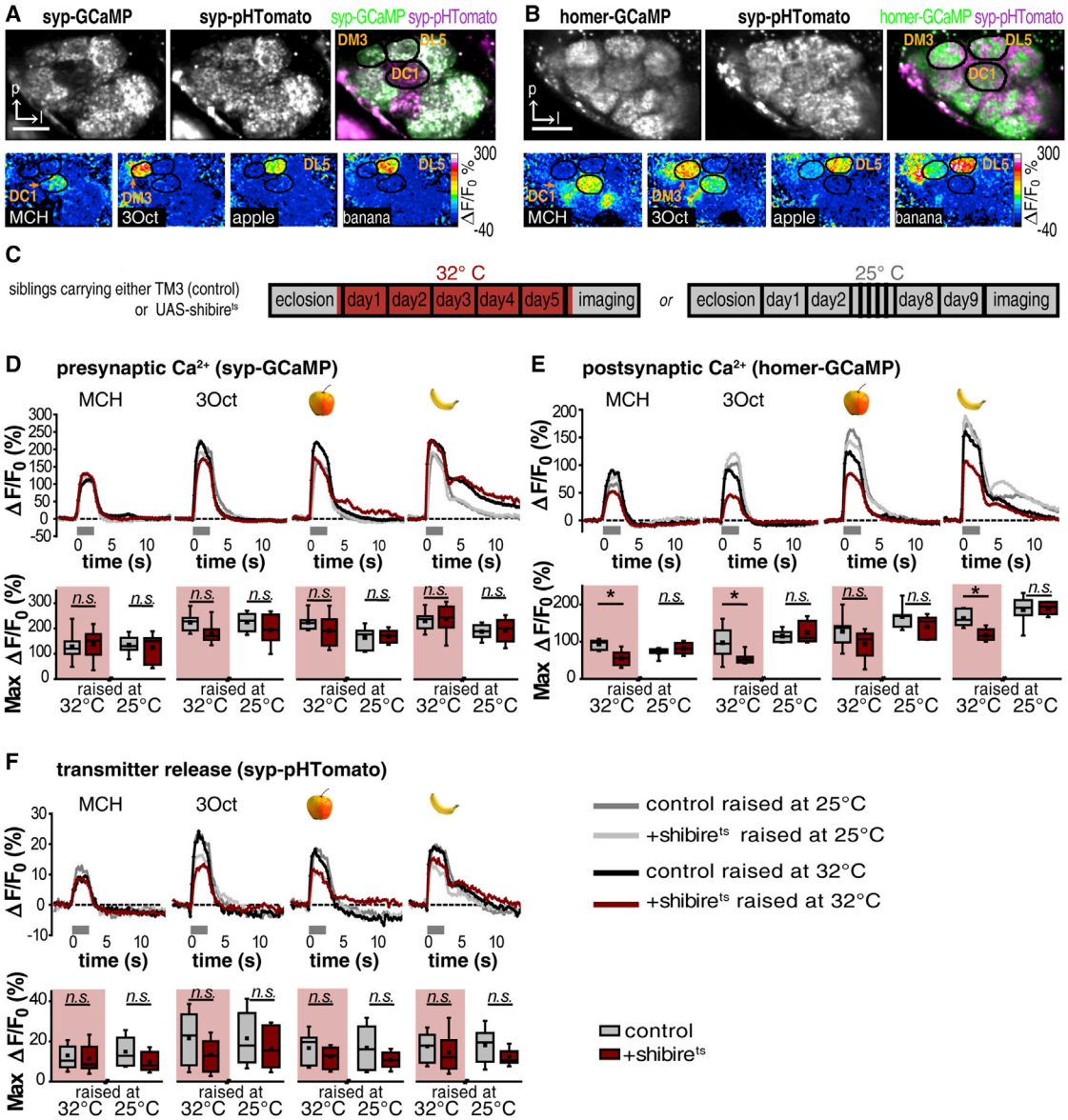

Figure 5. Activity-Dependent Plasticity of Postsynaptic Ca^{2+} in the AL

(A) In vivo fluorescence of syp-GCaMP (left) and syp-pHTomato (center) expressed together with $shibire^{ts}$ in OPNs. Glomeruli DC1, DM3, and DL5 show changes in fluorescence upon stimulation with MCH, 3Oct, apple, or banana odor, as shown in the bottom row for syp-GCaMP.

(B) In vivo fluorescence of homer-GCaMP (left) and syp-pHTomato (center) expressed together with $shibire^{ts}$ in OPNs. DC1, DM3, and DL5 show changes in fluorescence upon stimulation with MCH, 3Oct, apple, or banana odor, as shown in the bottom row for homer-GCaMP.

(C) Experimental protocol to study the effects of prolonged deprivation of transmission from OPNs. All flies express syp-pHTomato, along with either the pre- or the postsynaptic Ca^{2+} sensor in OPNs, and were imaged at 23°C.

(D) Odor-evoked changes in syp-GCaMP fluorescence in the four experimental groups in the glomeruli DC1 for MCH, DM3 for 3Oct, and DL5 for apple and banana odor (top row) and the respective comparison of the maximal fluorescence change during odor stimulation (bottom row). n = 6–8.

(E) Odor-evoked changes in homer-GCaMP fluorescence in the four experimental groups in DC1 for MCH, DM3 for 3Oct, and DL5 for apple and banana odor (top row) and the respective comparison of the maximal fluorescence change during odor stimulation (bottom row). n = 6–7.

(F) Dynamics and maximal change of simultaneously monitored syp-pHTomato fluorescence. Flies co-expressing either syp-GCaMP or homer-GCaMP were pooled; n = 12–15. All traces indicate mean values; box plots indicate medians, interquartile ranges, and 10%/90% range.

The scale bars represent 20 μm; *n.s.*, $p > 0.025$; *$p < 0.025$; two-sample t test.

amount of syp-GCaMP fluorescence per bouton, which suggests that the total number of vesicles per bouton was not altered (Figure 6E).

The differential changes in synaptic activity of OPNs induced by artificial deprivation mimic those induced by a natural experience. We exposed the animals for 5 days during early

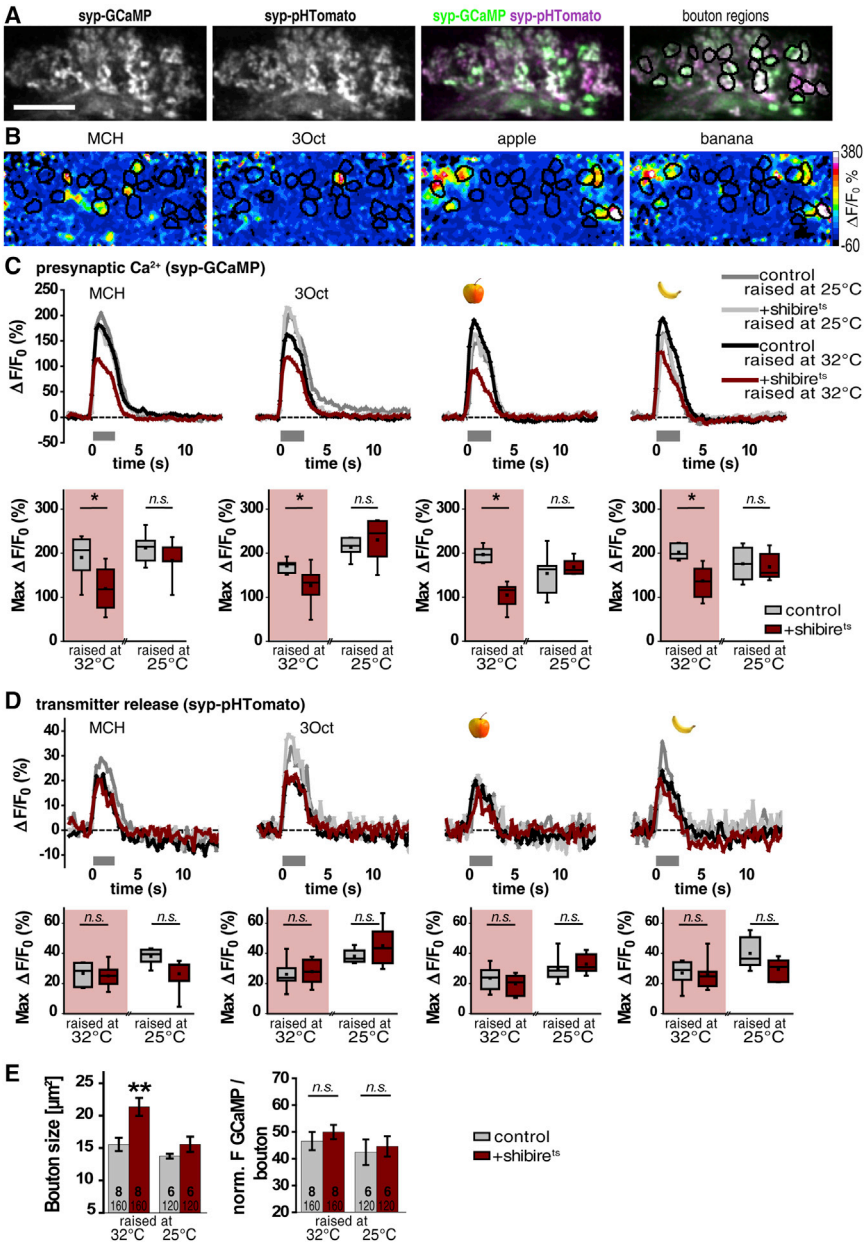

Figure 6. Activity-Dependent Plasticity of Presynaptic Ca^{2+} in the Calyx

(A and B) In vivo fluorescence in the calyx of a fly (A) that expresses both syp-GCaMP (left) and syp-pHTomato (center) in OPNs. Indicated by black lines are 20 bouton regions, some of which show fluorescence changes upon stimulation with either MCH, 3Oct, apple, or banana, as shown in (B) for syp-GCaMP.

(C) Dynamics of odor-evoked syp-GCaMP fluorescence in animals with or without shibire^{ts} expression and with or without prolonged maintenance at restrictive (32°C) or permissive (25°C) temperature. Dynamics of fluorescence changes in the most-responsive bouton for each odor (top row) and the respective maximal fluorescence change during odor stimulation (bottom row) are shown.

(D) Dynamics and maximal change of simultaneously monitored syp-pHTomato fluorescence. n = 6–8. Traces show mean values; box plots indicate medians, interquartile ranges, and 10%/90% range.

(E) Quantification of the bouton areas and the relative amount of GCaMP per bouton for the four experimental groups. Shown are the mean and SEM. Sample sizes of animals (bold) and of boutons (regular) are indicated within the bars.

The scale bars represent 20 μm; *n.s.*, $p > 0.025$; *$p < 0.025$; two-sample t test.

adulthood to a multimodal, including olfactory, cue by raising them on a piece of apple. This treatment typically causes behavioral adaptation and reduced responsiveness to the exposed odor (Sachse et al., 2007; Das et al., 2011). Subsequently, we compared odor responses of the respective sensors in these animals with odor responses in animals that were raised without apple (Figure 7A). We focused again on glomeruli DC1, DM3, and DL5 of the AL, using a dual color combination of either pre- or postsynaptic Ca^{2+} sensors and syp-pHTomato. As was the case in the artificial deprivation experiment, we did not observe any experience-dependent change in presynaptic Ca^{2+} signaling in the AL (Figure 7B). The amplitudes of postsynaptic Ca^{2+} transients, however, were clearly reduced in the apple-responsive glomerulus DL5 only in those animals that were raised on apple. In contrast to the deprivation experiment, this decrease in postsynaptic signaling induced by exposure to the apple odor was glomerulus specific. Syp-pHTomato signals of OPNs in the AL were also in this experiment unaltered (Figure 7D). We further repeated the experiment and compared flies that expressed either cytosolic or postsynaptically targeted GCaMP. We found that cytosolic-expressed GCaMP, in contrast to homer-GCaMP, did not report the DL5-specific reduction in postsynaptic Ca^{2+} (Figure S6). In conclusion, the localized sensor proteins are appropriate to optically dissect distinct parameters of synaptic signaling in pre- or postsynaptic compartments and to confine experience-dependent, synaptic plasticity to pre- and postsynaptic compartments.

DISCUSSION

Approaches to the detection of physiological parameters underlying synaptic functioning in real time, in vivo, and across many synapses are important for understanding the principles governing the ways in which neural circuits accomplish signal integration, learning, and memory. Presynaptically targeted GECIs

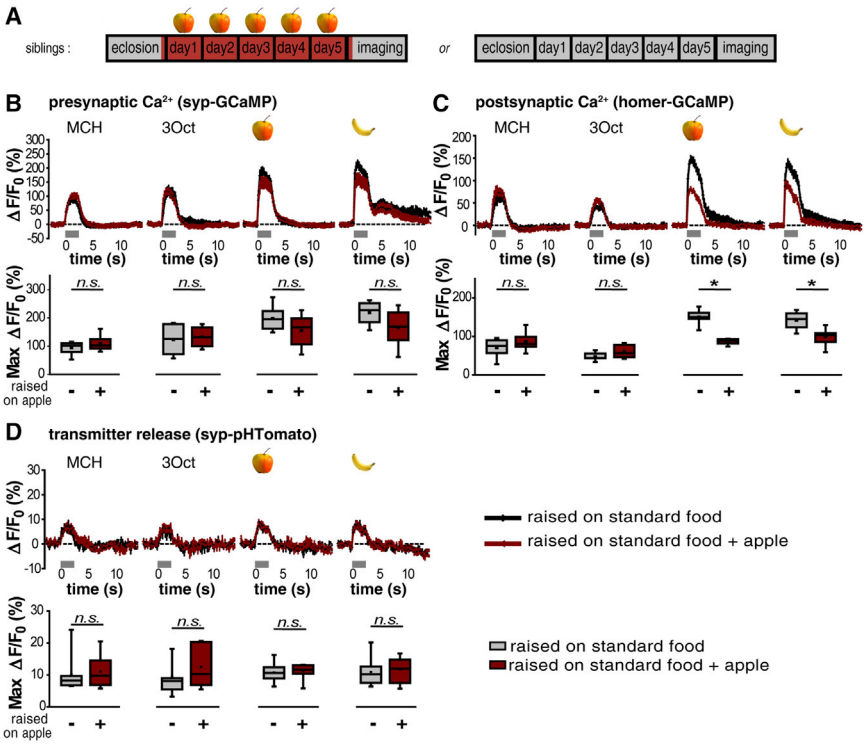

Figure 7. Experience-Dependent Plasticity of Postsynaptic Ca^{2+} in the AL

(A) Experimental protocol to study the effects of prolonged exposure to apple odor. All flies tested expressed syp-pHTomato along with either the pre- or the postsynaptic Ca^{2+} sensor in OPNs. Flies were transferred for 5 days to standard food containing 5 g of apple. A second group of siblings was raised on standard food only.

(B) Odor-evoked syp-GCaMP fluorescence changes of the two experimental groups in glomerulus DC1 for MCH, in DM3 for 3Oct, and in DL5 for apple and banana (top row) and the respective maximal fluorescence changes during odor stimulation (bottom row). n = 8.

(C) Odor-evoked homer-GCaMP fluorescence changes in DC1 for MCH, in DM3 for 3Oct, and in DL5 for apple and banana (top row) and the respective maximal fluorescence changes during odor stimulation (bottom row). n = 6–7.

(D) Odor-evoked syp-pHTomato fluorescence changes in DC1 for MCH, in DM3 for 3Oct, and in DL5 for apple and banana (top row) and the respective maximal fluorescence change during odor stimulation (bottom row). Flies co-expressing either syp-GCaMP or homer-GCaMP were pooled; n = 14–15. Traces show mean values and SEM; box plots indicate medians, interquartile ranges, and 10%/90% range.

n.s., $p > 0.05$; *$p < 0.05$; two-sample t test. See also Figure S6.

have been successfully used to monitor presynaptic Ca^{2+} signaling in vertebrate systems, (e.g., Dreosti et al., 2009; Zhao et al., 2011a; Li et al., 2011; Akerboom et al., 2012; Walker et al., 2013). Furthermore, synaptic transmission can be visualized using pH-sensitive fluorophores targeted to the lumen of synaptic vesicles (Miesenböck et al., 1998; Granseth et al., 2006; Zhu et al., 2009; Li and Tsien, 2012). Whereas Ca^{2+} dynamics are frequently monitored in the dendrites and postsynaptic spines of mammalian cultured neurons or brain sections (Denk et al., 1996; Oertner, 2002), specific sensors tagged to the postsynaptic density have not been described. So far, postsynaptic Ca^{2+} dynamics have been measured solely in muscle cells, at the neuromuscular junction of larval *Drosophila*. For this purpose, GECIs were introduced between the transmembrane domain of CD8 and the DLG-interacting domain of the K+ channel Shaker (Guerrero et al., 2005; Peled et al., 2014). Whereas *Drosophila* represents a key model organism to dissect the neuronal circuits that underlie stimulus processing and behavior (Venken et al., 2011), there is still a lack of efficient techniques to visualize synaptic activity in the brain. We generated transgenic fly lines to overcome these limitations.

First, presynaptic Ca^{2+} is detected using a synaptophysin-coupled GCaMP3 construct. Ca^{2+} has multiple functions in presynaptic terminals and also multiple locations, comprising high Ca^{2+} concentration nano- and microdomains around voltage-gated channels and more-global, intraterminal Ca^{2+} (Neher and Sakaba, 2008), and all contribute to the signals monitored using targeted GECIs. In vertebrate neurons, the molar quantity of Ca^{2+} and its spatial diffusion is highly variable among neurons and even among boutons of the same axon. In neocortical presynaptic boutons of different mammalian tissues, for example, action-potential-induced and volume-averaged Ca^{2+} changes cover an estimated range of peak concentrations from 300 nM to 1,000 nM (e.g., Koester and Sakmann, 2000; Dreosti et al., 2009; Vaithianathan and Matthews, 2014). The dynamic range (~100 nM–~10,000 nM) and K_D (~600 nM) of GCaMP3 (Tian et al., 2009) is within this concentration range. It should be noted, however, that the peak Ca^{2+} concentration at the active zone of some specialized synapses may exceed 10 μM (e.g., Bollmann et al., 2000). A very local saturation of GCaMP3 can, therefore, under respective experimental conditions, not be excluded. GCaMP3 shows a relatively strong baseline fluorescence compared to other recently reported GCaMP variants (Akerboom et al., 2012; Chen et al., 2013; Zhao et al., 2011b), which is crucial for the detection of the small and often dispersed structures in vivo (see also Mao et al., 2008). Second, we apply the red pHTomato coupled to Synaptophysin (Li and Tsien, 2012) to the central brain of *Drosophila*. This sensor is equally effective regarding presynaptic localization, relative changes in fluorescence, and signal-to-noise ratio when compared to synaptopHluorin that has been used in *Drosophila* (Ng et al., 2002). In response to physiological stimuli, amplitudes of fluorescence changes and signal to noise are small, however, due to the stochastic nature of exo- and endocytosis events and the small percentage of ready releasable vesicles (Sankaranarayanan et al., 2000, Denker et al., 2011). However, in combination with green fluorescent Ca^{2+} sensors, this sensor is helpful in identifying and differentiating pre- and postsynaptic compartments and in analyzing the physiological properties of synaptic function by correlating

synaptic vesicle release to synaptic Ca^{2+} influx. Third, we report homer-GCaMP as a postsynaptic Ca^{2+} sensor encompassing Ca^{2+} sources that can potentially derive from ligand-gated ionotropic receptors, voltage-gated Ca^{2+} channels of the postsynaptic membrane, or internal Ca^{2+} stores.

The olfactory pathway of the *Drosophila* central brain provides an advantageous test system due to the combinatorial nature of odor representations across anatomically and functionally well-characterized populations of neurons (Wilson, 2013). We demonstrate that the monitoring of pre- and postsynaptic Ca^{2+} dynamics is readily feasible, as is that of synaptic transmission across populations of synapses and within individual synaptic boutons. Experience-dependent plasticity of synaptic signaling in the AL has been proposed as a contributor to decreasing behavioral responsiveness following prolonged odor exposure (Sachse et al., 2007; Das et al., 2011), but tools to confirm this assumption have been lacking. Here, we show that the targeted sensors are appropriate to bridge that gap. The targeted sensors allow one not only to detect synaptic plasticity but also to tease apart experimentally the underlying signaling at the pre- and postsynapse within a complex circuit. The decrease in postsynaptic activity in OPNs caused by prolonged odor stimulation can be mimicked by artificially silencing OPN output. This indicates that olfactory adaptation is accompanied by a decrease in OPN activity, which might be mediated by plasticity of inhibitory local interneurons, as suggested by Das et al. (2011). This reduction of the postsynaptic Ca^{2+} in the AL is reflected by a reduction of presynaptic Ca^{2+} signaling in the CA, but not in the AL. Post- and presynaptic Ca^{2+} influxes in OPNs are, therefore, modulated independently. A large number of non-associative, associative, and complex learning paradigms have been described in *Drosophila*. The establishment of a method to monitor physiological parameters of synaptic activity in vivo in a largely intact animal provides a possibility to uncover synaptic plasticity underlying neuronal circuit processing and experience-dependent, adaptive behavior.

EXPERIMENTAL PROCEDURES

Generation of DNA Constructs and Transgenic Flies

The DNA of synaptophysin-GCaMP3 was obtained from S. Voglmaier and inserted into the pUAST vector. The DNA of pHTomato was obtained from Y. Li, cloned into the intravesicular domain of Synaptophysin, and inserted into pUAST. cDNA of *d*Homer was amplified from w1118 flies and inserted with a C-terminal-linked GCaMP3 into pUAST. A detailed description of procedures is provided in the Supplemental Experimental Procedures, along with a list of transgenic fly stocks used.

Immunohistochemistry

Brains of 3- to 6-day-old female flies or larval filets of third instar larvae were prepared and immunostained as described in detail in the Supplemental Experimental Procedures.

Confocal Imaging

Stacks of confocal images were generated using a confocal microscope (Leica) with a 20×/NA = 0.7 objective for whole brain scans and a 63×/NA = 1.4 objective for neuropils or larval motor neurons. A detailed description of image acquisition and analysis is provided in the Supplemental Experimental Procedures.

Two-Color STED Microscopy

Immunohistochemically stained brains were embedded in a polymer resin, cut into 50–60 nm sections, and imaged using a STED microscope (Leica) equipped with a 100×/NA = 1.4 oil immersion objective. Sample preparation was performed as described in Revelo et al. (2014), with modifications described in the Supplemental Experimental Procedures.

Wide-Field Imaging

Brains of female transgenic flies (5 days old) were imaged at 5 Hz through a window in the head capsule using a fluorescence microscope (Zeiss) equipped with a 20×/NA = 1 water-immersion objective. KCl was injected into the Ringer's solution covering the brain (final concentration ~0.05 M). Imaging and quantification of fluorescence changes are described in detail in the Supplemental Experimental Procedures.

Two-Photon Imaging

Stimulus-induced fluorescence changes in brain regions of female transgenic flies (3–6 days old) were imaged through a window in the head capsule at a frame rate of 4 or 5 Hz using a LSM 7MP two-photon microscope (Zeiss) equipped with a mode-locked Ti-sapphire laser (Coherent) and a 20×/NA = 1 water-immersion objective. All sensors were excited at 950 nm, and a dichroic mirror was combined with a 500- to 550-nm and a 575- to 610-nm BP filter to record GCaMP and pHTomato simultaneously. Imaging procedures, preparation, stimulus delivery, temperature control under the microscope, and image analysis is provided in the Supplemental Experimental Procedures.

Deprivation Experiments and Apple-Exposure Experiment

Detailed experimental protocols are provided in the Supplemental Experimental Procedures.

Behavioral Assays

Groups of ~20 third instar larvae were scored according to their chemotaxis toward an odor. Geotaxis was quantified in mixed populations of 20 flies, 4–6 days old, as described by Benzer (1967) with modifications described by Inagaki et al. (2010). Details for both assays are provided in the Supplemental Experimental Procedures.

FM Dye Experiments

Filets of third instar larvae were loaded with dye in high-potassium medium (see Supplemental Experimental Procedures for details) for 30 s, washed, and subsequently stimulated several times with 20-Hz trains of 100 mA for 10 s. Images of boutons at the neuromuscular junction were recorded and analyzed as described in the Supplemental Experimental Procedures.

Statistical Analysis

Data were tested for normal distribution using the Kolmogorov-Smirnov test. For comparing multiple groups, a one-way ANOVA was used. In the case of significance, the data were subjected to post hoc pairwise comparison using the two-sample Student's t test and p values were Bonferroni corrected. To test for difference to a fixed value, the Wilcoxon signed rank test was used. For determining the relation of $\Delta F/F_0$ values obtained from two wavelength channels, different models of the least square fit were compared by means of R^2 values, the Akaike information criterion (Akaike, 1974), and the Bayesian information criterion (Schwarz, 1978).

SUPPLEMENTAL INFORMATION

Supplemental Information includes Supplemental Experimental Procedures, six figures, and two movies and can be found with this article online at http://dx.doi.org/10.1016/j.celrep.2015.02.065.

AUTHOR CONTRIBUTIONS

A.F. and U.P. designed the study, interpreted the results, and wrote the manuscript. U.P. performed all experiments and analyzed the data, except for STED microscopy and FM dye experiments. N.H.R. and U.P. performed and

analyzed STED experiments, supervised by S.O.R. K.J.S. and S.O.R. performed and analyzed FM dye experiments. A.F. supervised the entire study.

ACKNOWLEDGMENTS

We thank Erich Buchner, Susan M. Voglmaier, Yulong Li, Stephen F. Heinemann, Hiromu Tanimoto, and Gero Miesenböck for providing fly strains, DNA constructs, or antibodies. We thank Tobias Mühmer, Jan Hoffmann, and Mandy Jauch for technical help and J. Böker and S. Castellón for assistance in fly care. This work was supported by the Deutsche Forschungsgemeinschaft (SFB 889/B04) and the German Ministry of Research and Education via the Bernstein Center for Computational Neuroscience Göttingen (01GQ1005A) to A.F. and by the European Research Council (ERC-2013-CoG NeuroMolAnatomy), the Deutsche Forschungsgemeinschaft (Cluster of Excellence Nanoscale Microscopy and Molecular Physiology of the Brain CNMPB and SFB889), and the Niedersachsen-Israeli Research Cooperation Program to S.O.R.

Received: October 15, 2014
Revised: January 24, 2015
Accepted: February 26, 2015
Published: March 26, 2015

REFERENCES

Akaike, H. (1974). A new look at the statistical model identification. IEEE Trans. Automat. Contr. *19*, 716–723.

Akerboom, J., Chen, T.W., Wardill, T.J., Tian, L., Marvin, J.S., Mutlu, S., Calderón, N.C., Esposti, F., Borghuis, B.G., Sun, X.R., et al. (2012). Optimization of a GCaMP calcium indicator for neural activity imaging. J. Neurosci. *32*, 13819–13840.

Benzer, S. (1967). BEHAVIORAL MUTANTS OF Drosophila ISOLATED BY COUNTERCURRENT DISTRIBUTION. Proc. Natl. Acad. Sci. USA *58*, 1112–1119.

Bollmann, J.H., Sakmann, B., and Borst, J.G. (2000). Calcium sensitivity of glutamate release in a calyx-type terminal. Science *289*, 953–957.

Brand, A.H., and Perrimon, N. (1993). Targeted gene expression as a means of altering cell fates and generating dominant phenotypes. Development *118*, 401–415.

Butcher, N.J., Friedrich, A.B., Lu, Z., Tanimoto, H., and Meinertzhagen, I.A. (2012). Different classes of input and output neurons reveal new features in microglomeruli of the adult Drosophila mushroom body calyx. J. Comp. Neurol. *520*, 2185–2201.

Chen, T.W., Wardill, T.J., Sun, Y., Pulver, S.R., Renninger, S.L., Baohan, A., Schreiter, E.R., Kerr, R.A., Orger, M.B., Jayaraman, V., et al. (2013). Ultrasensitive fluorescent proteins for imaging neuronal activity. Nature *499*, 295–300.

Christiansen, F., Zube, C., Andlauer, T.F., Wichmann, C., Fouquet, W., Owald, D., Mertel, S., Leiss, F., Tavosanis, G., Luna, A.J., et al. (2011). Presynapses in Kenyon cell dendrites in the mushroom body calyx of Drosophila. J. Neurosci. *31*, 9696–9707.

Das, S., Sadanandappa, M.K., Dervan, A., Larkin, A., Lee, J.A., Sudhakaran, I.P., Priya, R., Heidari, R., Holohan, E.E., Pimentel, A., et al. (2011). Plasticity of local GABAergic interneurons drives olfactory habituation. Proc. Natl. Acad. Sci. USA *108*, E646–E654.

Denk, W., Yuste, R., Svoboda, K., and Tank, D.W. (1996). Imaging calcium dynamics in dendritic spines. Curr. Opin. Neurobiol. *6*, 372–378.

Denker, A., Bethani, I., Kröhnert, K., Körber, C., Horstmann, H., Wilhelm, B.G., Barysch, S.V., Kuner, T., Neher, E., and Rizzoli, S.O. (2011). A small pool of vesicles maintains synaptic activity in vivo. Proc. Natl. Acad. Sci. USA *108*, 17177–17182.

Diagana, T.T., Thomas, U., Prokopenko, S.N., Xiao, B., Worley, P.F., and Thomas, J.B. (2002). Mutation of Drosophila homer disrupts control of locomotor activity and behavioral plasticity. J. Neurosci. *22*, 428–436.

Dreosti, E., Odermatt, B., Dorostkar, M.M., and Lagnado, L. (2009). A genetically encoded reporter of synaptic activity in vivo. Nat. Methods *6*, 883–889.

Granseth, B., Odermatt, B., Royle, S.J., and Lagnado, L. (2006). Clathrin-mediated endocytosis is the dominant mechanism of vesicle retrieval at hippocampal synapses. Neuron *51*, 773–786.

Grienberger, C., and Konnerth, A. (2012). Imaging calcium in neurons. Neuron *73*, 862–885.

Guerrero, G., Reiff, D.F., Agarwal, G., Ball, R.W., Borst, A., Goodman, C.S., and Isacoff, E.Y. (2005). Heterogeneity in synaptic transmission along a Drosophila larval motor axon. Nat. Neurosci. *8*, 1188–1196.

Inagaki, H.K., Kamikouchi, A., and Ito, K. (2010). Methods for quantifying simple gravity sensing in Drosophila melanogaster. Nat. Protoc. *5*, 20–25.

Kitamoto, T. (2001). Conditional modification of behavior in Drosophila by targeted expression of a temperature-sensitive shibire allele in defined neurons. J. Neurobiol. *47*, 81–92.

Koester, H.J., and Sakmann, B. (2000). Calcium dynamics associated with action potentials in single nerve terminals of pyramidal cells in layer 2/3 of the young rat neocortex. J. Physiol. *529*, 625–646.

Kremer, M.C., Christiansen, F., Leiss, F., Paehler, M., Knapek, S., Andlauer, T.F., Förstner, F., Kloppenburg, P., Sigrist, S.J., and Tavosanis, G. (2010). Structural long-term changes at mushroom body input synapses. Curr. Biol. *20*, 1938–1944.

Kuromi, H., and Kidokoro, Y. (1999). The optically determined size of exo/endo cycling vesicle pool correlates with the quantal content at the neuromuscular junction of Drosophila larvae. J. Neurosci. *19*, 1557–1565.

Leiss, F., Groh, C., Butcher, N.J., Meinertzhagen, I.A., and Tavosanis, G. (2009). Synaptic organization in the adult Drosophila mushroom body calyx. J. Comp. Neurol. *517*, 808–824.

Leube, R.E. (1995). The topogenic fate of the polytopic transmembrane proteins, synaptophysin and connexin, is determined by their membrane-spanning domains. J. Cell Sci. *108*, 883–894.

Li, Y., and Tsien, R.W. (2012). pHTomato, a red, genetically encoded indicator that enables multiplex interrogation of synaptic activity. Nat. Neurosci. *15*, 1047–1053.

Li, H., Foss, S.M., Dobryy, Y.L., Park, C.K., Hires, S.A., Shaner, N.C., Tsien, R.Y., Osborne, L.C., and Voglmaier, S.M. (2011). Concurrent imaging of synaptic vesicle recycling and calcium dynamics. Front. Mol. Neurosci. *4*, 34.

Mao, T., O'Connor, D.H., Scheuss, V., Nakai, J., and Svoboda, K. (2008). Characterization and subcellular targeting of GCaMP-type genetically-encoded calcium indicators. PLoS One *3*, e1796.

Miesenböck, G., De Angelis, D.A., and Rothman, J.E. (1998). Visualizing secretion and synaptic transmission with pH-sensitive green fluorescent proteins. Nature *394*, 192–195.

Neher, E., and Sakaba, T. (2008). Multiple roles of calcium ions in the regulation of neurotransmitter release. Neuron *59*, 861–872.

Ng, M., Roorda, R.D., Lima, S.Q., Zemelman, B.V., Morcillo, P., and Miesenböck, G. (2002). Transmission of olfactory information between three populations of neurons in the antennal lobe of the fly. Neuron *36*, 463–474.

Oertner, T.G. (2002). Functional imaging of single synapses in brain slices. Exp. Physiol. *87*, 733–736.

Peled, E.S., Newman, Z.L., and Isacoff, E.Y. (2014). Evoked and spontaneous transmission favored by distinct sets of synapses. Curr. Biol. *24*, 484–493.

Revelo, N.H., Kamin, D., Truckenbrodt, S., Wong, A.B., Reuter-Jessen, K., Reisinger, E., Moser, T., and Rizzoli, S.O. (2014). A new probe for super-resolution imaging of membranes elucidates trafficking pathways. J. Cell Biol. *205*, 591–606.

Riemensperger, T., Pech, U., Dipt, S., and Fiala, A. (2012). Optical calcium imaging in the nervous system of Drosophila melanogaster. Biochim. Biophys. Acta *1820*, 1169–1178.

Sachse, S., Rueckert, E., Keller, A., Okada, R., Tanaka, N.K., Ito, K., and Vosshall, L.B. (2007). Activity-dependent plasticity in an olfactory circuit. Neuron *56*, 838–850.

Sankaranarayanan, S., De Angelis, D., Rothman, J.E., and Ryan, T.A. (2000). The use of pHluorins for optical measurements of presynaptic activity. Biophys. J. *79*, 2199–2208.

Schwarz, G. (1978). Estimating the dimension of a model. Ann. Stat. *6*, 461–464.

Silbering, A.F., Okada, R., Ito, K., and Galizia, C.G. (2008). Olfactory information processing in the Drosophila antennal lobe: anything goes? J. Neurosci. *28*, 13075–13087.

Stocker, R.F., Heimbeck, G., Gendre, N., and de Belle, J.S. (1997). Neuroblast ablation in Drosophila P[GAL4] lines reveals origins of olfactory interneurons. J. Neurobiol. *32*, 443–456.

Tantama, M., Hung, Y.P., and Yellen, G. (2012). Optogenetic reporters: Fluorescent protein-based genetically encoded indicators of signaling and metabolism in the brain. Prog. Brain Res. *196*, 235–263.

Tian, L., Hires, S.A., Mao, T., Huber, D., Chiappe, M.E., Chalasani, S.H., Petreanu, L., Akerboom, J., McKinney, S.A., Schreiter, E.R., et al. (2009). Imaging neural activity in worms, flies and mice with improved GCaMP calcium indicators. Nat. Methods *6*, 875–881.

Vaithianathan, T., and Matthews, G. (2014). Visualizing synaptic vesicle turnover and pool refilling driven by calcium nanodomains at presynaptic active zones of ribbon synapses. Proc. Natl. Acad. Sci. USA *111*, 8655–8660.

Venken, K.J., Simpson, J.H., and Bellen, H.J. (2011). Genetic manipulation of genes and cells in the nervous system of the fruit fly. Neuron *72*, 202–230.

Wagh, D.A., Rasse, T.M., Asan, E., Hofbauer, A., Schwenkert, I., Dürrbeck, H., Buchner, S., Dabauvalle, M.C., Schmidt, M., Qin, G., et al. (2006). Bruchpilot, a protein with homology to ELKS/CAST, is required for structural integrity and function of synaptic active zones in Drosophila. Neuron *49*, 833–844.

Walker, A.S., Burrone, J., and Meyer, M.P. (2013). Functional imaging in the zebrafish retinotectal system using RGECO. Front. Neural Circuits *7*, 34.

Wilson, R.I. (2013). Early olfactory processing in Drosophila: mechanisms and principles. Annu. Rev. Neurosci. *36*, 217–241.

Wilson, R.I., Turner, G.C., and Laurent, G. (2004). Transformation of olfactory representations in the Drosophila antennal lobe. Science *303*, 366–370.

Wong, A.M., Wang, J.W., and Axel, R. (2002). Spatial representation of the glomerular map in the Drosophila protocerebrum. Cell *109*, 229–241.

Xiao, B., Tu, J.C., Petralia, R.S., Yuan, J.P., Doan, A., Breder, C.D., Ruggiero, A., Lanahan, A.A., Wenthold, R.J., and Worley, P.F. (1998). Homer regulates the association of group 1 metabotropic glutamate receptors with multivalent complexes of homer-related, synaptic proteins. Neuron *21*, 707–716.

Yasuyama, K., Meinertzhagen, I.A., and Schürmann, F.W. (2002). Synaptic organization of the mushroom body calyx in Drosophila melanogaster. J. Comp. Neurol. *445*, 211–226.

Zhao, C., Dreosti, E., and Lagnado, L. (2011a). Homeostatic synaptic plasticity through changes in presynaptic calcium influx. J. Neurosci. *31*, 7492–7496.

Zhao, Y., Araki, S., Wu, J., Teramoto, T., Chang, Y.F., Nakano, M., Abdelfattah, A.S., Fujiwara, M., Ishihara, T., Nagai, T., and Campbell, R.E. (2011b). An expanded palette of genetically encoded Ca^{2+} indicators. Science *333*, 1888–1891.

Zhu, Y., Xu, J., and Heinemann, S.F. (2009). Two pathways of synaptic vesicle retrieval revealed by single-vesicle imaging. Neuron *61*, 397–411.